PAPER

Determination of q during sawtooth from inverse evolution of BAEs in Tore Supra

IOP Publishing | International Atomic Energy Agency Nuclear Fusion

Nucl. Fusion **58** (2018) 016010 (8pp) https://doi.org/10.1088/1741-4326/aa85a9

Determination of q during sawtooth from inverse evolution of BAEs in Tore Supra

C.H.S. Amador[1,2], R. Sabot[2], X. Garbet[2], Z.O. Guimarães-Filho[3] and J.-H. Ahn[2]

[1] Departamento de Ciências da Natureza, Universidade Tecnológica Federal do Paraná, 86300-000, Cornélio Procópio, Paraná, Brazil
[2] CEA, IRFM, F-13108 Saint-Paul-lez-Durance, France
[3] Institute of Physics, University of São Paulo, 05508-090 São Paulo, São Paulo, Brazil

E-mail: cassioamador@utfpr.edu.br

Received 9 January 2017, revised 2 August 2017
Accepted for publication 11 August 2017
Published 6 November 2017

Abstract

Measuring the value of the safety factor (q) in the core during sawtooth cycles is still an open issue. A new method to measure q in Tore Supra plasma core is presented here. It relies on the analysis of the time evolution of a set of MHD modes detected after the sawtooth crashes. These modes are in the frequency range of previously observed Beta-induced Alfvén Eigenmodes, but with a frequency declining in time. The mode frequency analysis shows that the q profile is reversed when we have ICRH, after the sawtooth crash. In high current discharges ($I_p > 1.15$ MA), the q-profile remains reversed for a longer time compared with lower plasma current discharges. Non-linear 3D MHD simulations of sawteeth performed with the XTOR-2F code (Lütjens and Luciani 2010 *J. Comput. Phys.* **229** 8130–43) exhibit features that are similar to these observations.

Keywords: magnetohydrodynamic waves, reflectometry, q profile measurement

(Some figures may appear in colour only in the online journal)

1. Introduction

One of the key parameters for tokamak operation and plasma characterization is the safety factor. This factor measures the winding of the field lines around the torus, and it is given by [2]:

$$q = \frac{\vec{B} \cdot \nabla \varphi}{\vec{B} \cdot \nabla \theta} \quad (1)$$

where $\vec{B}$ is the magnetic field, φ and θ are the toroidal and poloidal angles, respectively. The evolution of the safety factor radial profile, also known as the q profile, during a sawtooth cycle in tokamaks has been a subject of discussion since the first observation of sawteeth by von Goeler *et al* in 1974 [3]. The first reconnection model proposed by Kadomtsev in 1975 [4] describes a basic mechanism for the sawtooth instability as an internal kink mode with $m = n = 1$ (m and n are poloidal and toroidal numbers) which develops and grows in the plasma core. During this process, the central q value (q_0) remains below 1, until a reconnection ends [5, 6]. Just after the reconnection, the q profile is flat, and $q \approx 1$ from the magnetic axis up to the inversion radius. The crash also flattens the core temperature and density profiles. Subsequent developments taking account the role of fast particles [5, 7], as well as alternative models (see Hastie's review [8]), have been proposed to explain the sawtooth instability. Prediction about the q profile value and its time evolution could differ strongly—some models requiring an almost flat $q = 1$ profile, others predicting partial reconnection with $q < 1$ after the crash.

The first measurements of the core q profile during sawtooth phenomena were performed on TEXTOR with Faraday rotation diagnostic [9]. Soltwisch *et al* reported a q_0 value well below $q = 1$ over the full sawtooth periods. These measurements were confirmed on DIII-D [10] and TFTR [11] using motional Stark effect (MSE) diagnostic and then on JET [12]. In each case q_0 remains around 0.75 and increase slightly (around 5%) at each crash before slowly declining. Observation of snakes [13], ie a high density closed tube of plasma that survives several sawtooth crashes, were seen as

another clue contradicting Kadomtsev's full reconnection model.

In opposition with these results, q profile evolution above and below $q = 1$ were also reported. Using MSE measurements with radial electric field correction, Rice *et al* [14] reported that q_0 remains close to one on DIII-D, dropping to $0.9 - 0.95$ before a sawtooth crash and returning to near unity after the crash.

High velocity pellet injections were also used to get information on the q profile [15]. The large dip in the pellet light emission when crossing the $q = 1$ surface was interpreted as evidence of a local flattening of the q profile [16, 17], with a local shear value at least one order of magnitude lower than the expected value assuming a parabolic q profile. Because of these contradictory results, the evolution of the q profile during sawteeth is still debated.

Information on the q profile can also be retrieved from the detection and evolution of MHD modes. Magnetohydrodynamics (MHD) spectroscopy relies on the q dependence of Alfvén eigenmodes (AEs) excited by external antennas or by energetic particles to improve q profile reconstruction from magnetic equilibrium [18]. In reverse shear discharges, the q-profile is hollow, and exhibits a minimum value, $q_{\min}$, larger than 1. In discharges with supra-thermal ion populations, frequency sweeping AEs can be excited. Dubbed Alfvén cascades, or reversed shear AEs (RSAEs), they exhibit upward frequency sweeping more commonly [19, 20]. Each cascade consists of several modes. From the dynamic of the Alfvén cascades, the time when $q_{\min}$ crosses a low rational surface such as $q = 3/2$ or $q = 2$ can be recovered.

In this work we will show that the set of downward chirping modes observed just after the sawtooth crash in Tore Supra ICRH discharges follow the Alfvén cascades equation. Applying MHD spectroscopy techniques, the q profile evolution just after a sawtooth crash will thus be recovered from MHD mode observation for the first time in Tore Supra. In the next section, the MHD spectroscopy method is described. In section 3, previous observations of modes in the acoustic frequency range in ICRH sawtooth discharges are recalled. In section 4, observations in low and high current discharges are presented. The modes detected just after the crash are identified in section 5, and the q-profile evolution is presented. In section 6, the q profile evolution from non-linear MHD simulations with the XTOR-2F code [1] is shown to support the observation both for low and high current discharges.

2. Alfvén cascades

Reversed shear shots can be created when additional heating produces fast ions, for example when there is the presence of NBI or ICRH. Reversed q profiles exhibit a minimum value, $q_{\min}$, larger than 1 (for example $q = 3/2$ or $q = 2$), which can be evaluated through its relation with the frequency of AE that grow in the plasma. The modes that appear in this situation are called the Reversed Shear AEs, and, in the case that the shear is low (q close to 1), we can have Alfvén cascades [21], as observed in JET [20, 22], driven by energetic ions. The mode frequency is given by the following equation:

$$f_{\mathrm{AC}} = \left| n - \frac{m}{q_{\min}} \right| f_{\mathrm{A}} + \delta f \tag{2}$$

where δf is a shift frequency, related to the plasma rotation, and f_{A} is the Alfvén frequency:

$$f_{\mathrm{A}} = \frac{B}{R\sqrt{\mu_0 n_{\mathrm{i}} m_{\mathrm{i}}}} \tag{3}$$

where μ_0 is the vacuum magnetic permeability, n_{i} and m_{i} are the ionic density and mass, respectively, and B is the total magnetic field in the cutoff position. The values of m and n are measured with magnetic diagnostics, so if the frequency evolution of the measured modes is fitted with this equation, $q_{\min}$ can be found, which consists in the technique of MHD spectroscopy. This technique was also applied on ASDEX Upgrade [23, 24], with a NBI heated plasma. The equation (2) had to be modified, because these MHD modes occurred in the acoustic wave range [25]:

$$f_{\mathrm{AC}} = \sqrt{{f_{\mathrm{S}}}^2 + \left(\left| n - \frac{m}{q_{\min}} \right| f_{\mathrm{A}} \right)^2} + \delta f \tag{4}$$

where f_{S} is an acoustic frequency, and δf was considered to be the toroidal rotation frequency times n, to account for Doppler shift from plasma to laboratory frame. This equation turns to equation (2) when $f_{\mathrm{S}} \ll \left| n - \frac{m}{q_{\min}} \right| f_{\mathrm{A}}$.

3. Observation of BAEs in Tore Supra

In Tore Supra, ion cyclotron resonance heating (ICRH) was the main heating source accelerating ions. In ICRH discharges, AEs were routinely detected [26]. Modes in the acoustic frequency range were identified as the so-called Beta-induced AEs (BAEs) [21, 27–31]. The physics of BAEs has been studied extensively [26], [32–35]. In pure ICRH discharges, the condition for BAE observation agreed well with the predicted ICRH power threshold (as shown in figure 12 of [32]). The mode frequency also followed the prediction:

$$f_{\mathrm{BAE}} = \frac{1}{R}\sqrt{\frac{2T_{\mathrm{i}}}{m_{\mathrm{i}}}\left(\frac{7}{4} + \frac{T_{\mathrm{e}}}{T_{\mathrm{i}}}\right)} \tag{5}$$

where m_{i} is the ion mass, T_{i} and T_{e} are the ion and electron temperatures.

In ICRH discharges with sawteeth, several modes in the acoustic frequency range could be observed after the sawtooth crash, before merging in a single mode toward the end of the sawtooth cycle (figure 3 from [35]). Guimarães-Filho showed that these modes exhibit different poloidal numbers, as shown by the opposite poloidal parity for adjacent modes. Their radial position was also studied. The position of the temperature fluctuation of the strongest mode was shown to slowly drift inwards during the sawtooth cycle. Assuming the mode to remain on the same rational surface, this inward drift would be incompatible with a monotonic q profile. q profile evolution according to the Kadomtsev model would produce an outward drift of resonant surfaces during the sawtooth ramp. A very flat or a reverse q profile would, rather, be consistent with an

Table 1. Shot parameters.

Shot	I_p (MA)[a]	ICRH(MW)	R (m)[b]	r (m)[c]	Shaf. shift (m)[d]	ε[e]	Inv. rad./r[f]
#47413 [g]	1.25	2.09	2.32	0.69	0.06	1.05	0.3
#41926	0.95	3.41	2.39	0.72	0.08	1	0.24

[a] Plasma current.
[b] Major radius.
[c] Minor radius.
[d] Shafranov shift.
[e] Plasma ellipticity.
[f] Normalized inversion radius with minor radius, considering the Shafranov shift.
[g] First reflectometer trigger, during high current.
[h] First reflectometer trigger, during low current.

inward mode drift during the sawtooth rise. It was then suggested that the observation of RSAE would be an indication confirming this hypothesis [35].

4. Observations of modes for different plasma currents

To investigate the nature of the modes reported by Guimarães-Filho *et al* ICRH discharges with BAE activity were analyzed. ICRH can produce fast ions in localized regions, so not all shots with this heating system are suitable. We selected discharges where the reflectometry diagnostic probed the core at fixed frequency for at least 1 full sawtooth cycle (in between two crashes, usually from 10 to 20 ms). The fluctuation reflectometry diagnostic has two channels (two different frequencies at the same time), with a 1 MHz acquisition rate, and heterodyne detection [36]. Triggers can be set at different moments of the discharge, so that more plasma environments can be studied during the same discharge [36].

The signal from these two reflectometry channels can be cross-correlated, and also correlated with the fast interferometry diagnostic signals (1 MHz of acquisition rate as well) [37]. More specifically, we used the lines that cross the core, to be able to distinguish between modes with different spatial structures. The fast electron cyclotron emission (ECE) diagnostic was not used because in these discharges it could not discriminate the fine details of each mode above 20 kHz [35].

Two discharges were analyzed in details, with their parameters detailed in table 1. High plasma current can lower the values for the q profile at the edge, which increases the area of $q = 1$. This can be observed via the value of the inversion radius for each case.

The spectrograms from the reflectometry signals, for both channels in these discharges, are shown in figures 1 and 2. The phase shift between each mode was evaluated by cross-correlating the fast interferometry and the reflectometry signals, as in figure 3 for shot #47413. This technique allows one to compare the phase of the detected modes by two different diagnostics (more details in [38]). The phase variation between modes shows that they are not in phase; hence, their spatial structure (the poloidal, m, and the toroidal, n, mode numbers) must be different.

The pattern in the spectrograms can be divided in two stages, delimited by the time of the modes frequency crossover. The first stage, with a chirping before the crossover, is only observed in shot #47413. An evaluation of the frequency difference between adjacent modes shows that it is not constant for all modes, in time. So the frequencies cannot have a linear dependence on m ($f = f_0 + mf_1$, with both f_0 and f_1 being time dependent). Also, it is possible to observe that the frequency modes do not cross each other at the same time, which could only happen if there was a time that $f = f_0$, for any given f_1, another indication that the modes are not linear with m. As figure 1 shows, the stage before the crossover is not always observed—an indication that it may be very sensitive to sawtooth reconnection dynamic or radial position.

The second part, after the chirping, is present in both shots shown here. In this stage, the frequency shifts between adjacent modes are almost constant, implying a possible frequency given by $f = f_0 + mf_1$.

5. Identification of the modes

The modes described in the previous section seem to be related to a profile with reverse shear, because the mode frequencies decrease right after the crash, and then start to increase, which could be related with a $q_{\min}$ changing from a value larger than 1 to 1. So in this case we are in the limit of low shear of the q profile, and we can expect to find Alfvén cascades [21], and we can use the RSAE equation (4) to fit the mode frequencies. We assumed δf to be the toroidal rotation times the toroidal mode number, plus the diamagnetic frequency times the poloidal number, to account for the mode rotation, changing the equation frame of reference to the laboratory frame. From sawtooth models, $n = m$ is expected [8], so the equation becomes:

$$f = \sqrt{{f_{\mathrm{BAE}}}^2 + \left(m\left|1 - \frac{1}{q_{\min}}\right| f_{\mathrm{A}}\right)^2} + m(f_{\mathrm{Tor}} + f_{\mathrm{dia}}). \qquad (6)$$

The measurement uncertainties in the various terms prevent direct comparison with the frequency measurements. In addition to the uncertainty on the cutoff position, the discrete nature of the measurements of both temperature and density profiles lead to uncertainties of several percent leading to several kHz for the BAE (equation (5)) and Alfvén frequencies. The same uncertainty level affects the diamagnetic frequency. Moreover, in this shot, toroidal rotation frequency was not measured, although for similar Tore Supra discharges x-ray

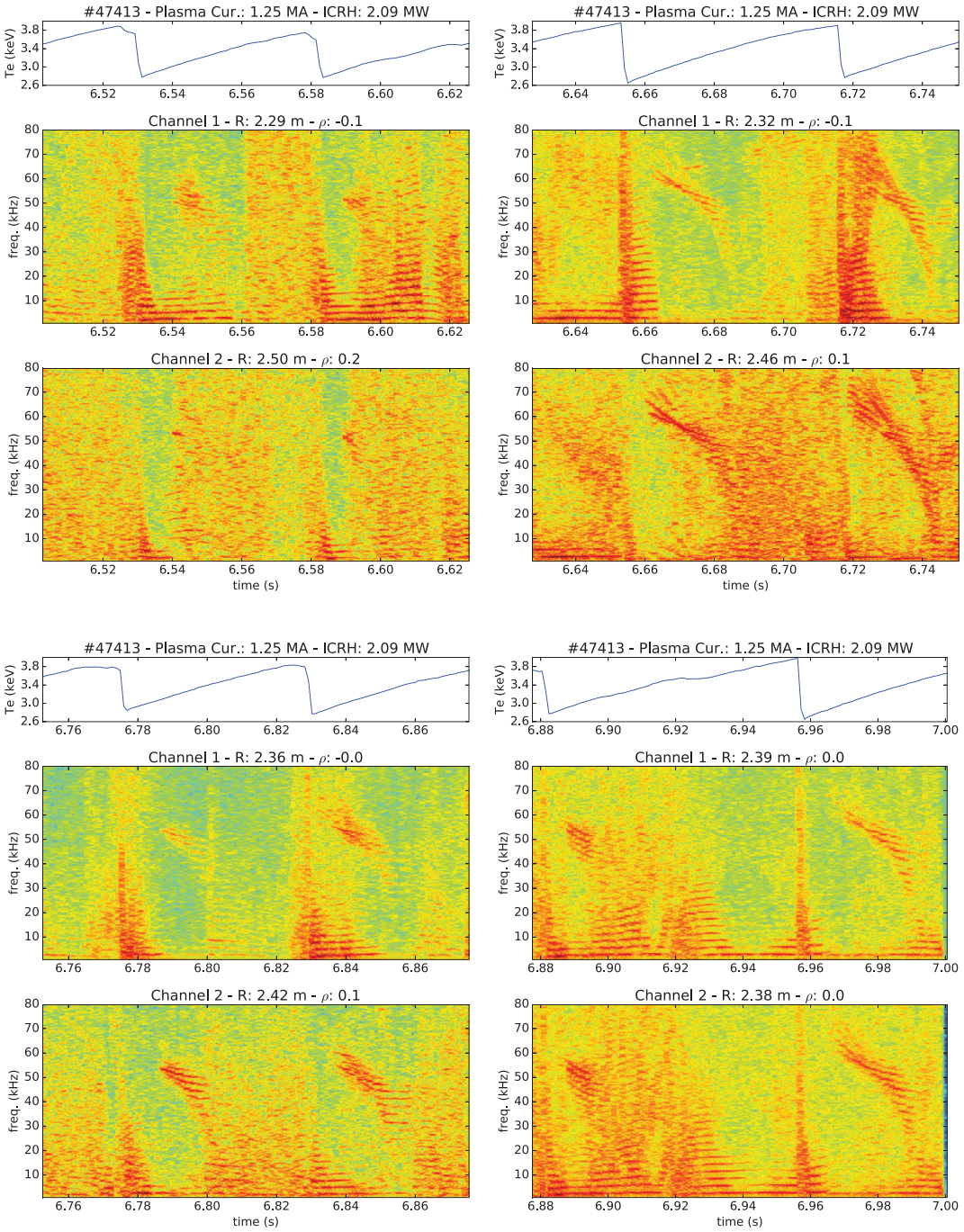

Figure 1. Spectrograms from both fixed frequency reflectometry diagnostic channels, for different positions, on adjacent sawteeth crashes, for discharge #47413.

crystal spectrometry estimates the toroidal rotation frequency close to 2 kHz [39]. Also, it is possible to estimate the rotation by the fast ECE data.

Because of these inaccuracies, equation (6) was fitted with a three parameter formula:

$$f = \sqrt{{f_0}^2 + (mf_1)^2} + mf_2 \tag{7}$$

where:

$$f_0 = f_S \tag{8}$$

$$f_1 = \left|1 - \frac{1}{q_{\min}}\right| f_A \tag{9}$$

$$f_2 = f_{\mathrm{Tor}} + f_{\mathrm{dia}}. \tag{10}$$

We can consider that the plasma rotation, in what concerns the frame of reference, has a slow change compared with one sawtooth, so we considered the parameter f_2 to be constant in time, with a value that can be estimated from fast ECE data, and also the aforementioned x-ray crystal spectrometry, to be $f_2 = -2.8$ kHz. The minus sign come from the modes

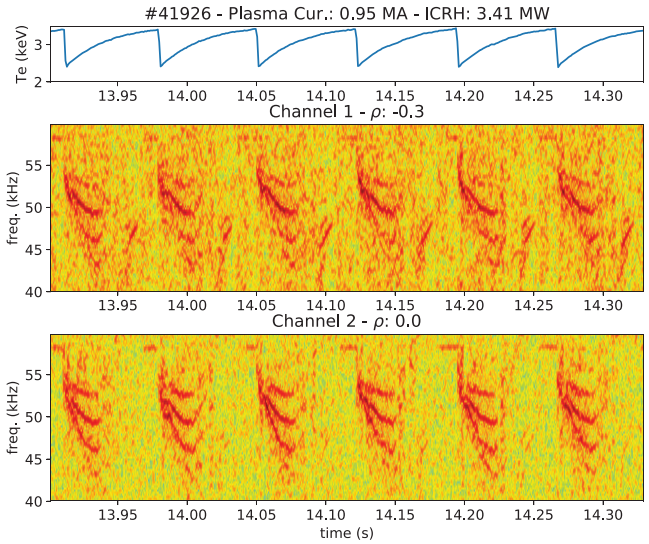

Figure 2. Spectrograms from both fixed frequency reflectometry diagnostic channels, for different positions, on adjacent sawteeth crashes, for discharge #41926.

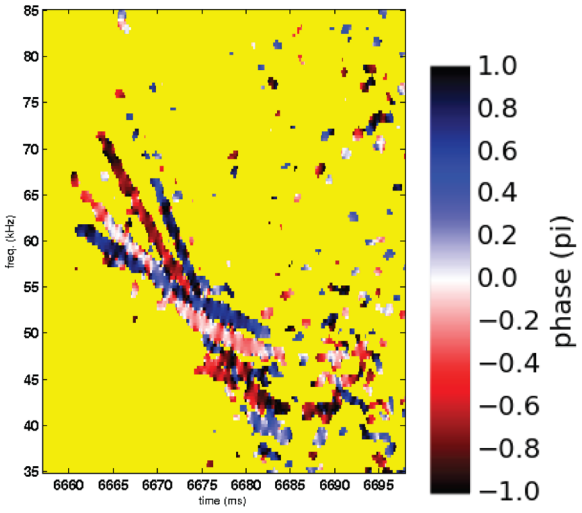

Figure 3. Phase spectrogram from cross-correlation between reflectometry and interferometry signals. Each mode shows a different phase shift, indicating different spatial structures (mainly poloidal and toroidal mode numbers). The yellow color corresponds to frequency regions with low spectral power.

observed in the spectrograms considered here, so we can suppose that the m value increases as the frequency of the mode decreases. Any deviation of the real rotation frequency from this estimated value will affect mainly the absolute value of parameter f_0, without changing its behavior in time.

The other restrained parameters are the $m = n$ values, which, in Tore Supra, cannot be evaluated from other diagnostics. We know, from figure 3, that it increases in odd numbers for each line. For simplicity, we choose it to be $m = 1, 2, 3, ...$, which adds an uncertainty in the absolute value of the fitted parameters, especially f_0, but it also does not change its temporal evolution behavior. Denoting the difference of the first m value from the real value as Δm, the value of f_0 should increase approximately by $\Delta m|f_2|$, if Δm is small. For example, if $m = 3, 4, 5...$—in other words, if there is a $\Delta m = 2$ for the first value—f_0 should increase by 5.6 kHz.

Considering f_2 fixed, it is possible to find the frequencies f_0 and f_1 in time, through a least square minimization, from the available data of the detected modes, for each sawtooth. No regularization constraints were applied, which explain the small oscillations in time, and here we see their absolute values, because equation (7) does not make it possible to determine their sign. To compare the fitted parameters between each sawtooth, we consider their mechanics to be approximately the same, so it is possible to map the time to a relative scale, where $t_{rel} = 0$ and $t_{rel} = 1$ represent the times of the previous and the next crash, respectively. For the shot #47413, there are two sawteeth probed for each position (figure 1), and we can retrieve the modes from sawtooth 3 to 8. We can compare these results with the discharge with the low plasma current case (#41926). The reflectometer channels in shot #41926 have 6 sawteeth for the same probed position. The results are in figure 4), and their dispersion shows that, although we can have variations for each crash, the general behavior is the same for the sawteeth in each discharge.

The first parameter, $|f_0|$, is related to the BAE acoustic frequency from equation (5). The values are close to the estimated BAE frequency: on average, f_{BAE} should be around 60 kHz in Tore Supra. However, for both shots, $|f_0|$ decreases in time, whereas from the BAE equation a frequency rise is expected, since the temperature increases after the crash. This deviation may be interrelated with the role of fast ions after the crash, since equation (5) is a first order approximation that does not take into account higher order corrections [32, 40]. These results were also observed in [41], which discuss in detail the effects of fast ions on the BAE frequency, showing results from LIGKA software simulations, that exhibits a decrease in BAE frequency in time.

q_{min} can be evaluated from the second parameter, $|f_1|$, since $|f_1|/f_A = 1 - (1/q_{min})$, f_A being the alfvénic frequency. As discussed before, the absolute value can change depending on the chosen m values, but, nevertheless, we can follow and compare the evolution of q_{min} in time, shown in figure 5.

The evolution of q_{min} depends on the sign of $|f_1|$, considered here to be positive, since this will lead to a decrease in q_{min} during the recovery phase in between crashes. This is related to the increase in temperature, which causes a decrease in resistivity, which leads to an increase of the current density, and therefore a decrease of q_{min}.

The evolution of q_{min} indicates that after the crash, it is higher than 1, and it decreases until reaching $q = 1$. For the discharge #41926, this parameter goes faster to unity if compared with shot #47413, which also has a higher post-crash value. This behavior is consistent through all sawteeth studied. When $q_{min} = 1$, equation (11) turns into:

$$f = f_S + m(f_{Tor} + f_{dia}) \tag{11}$$

which would represent equally displaced modes, as it is observed at the end period of all the modes shown in this work. A similar expression was proposed in [38], based on the behavior of the mode evolution.

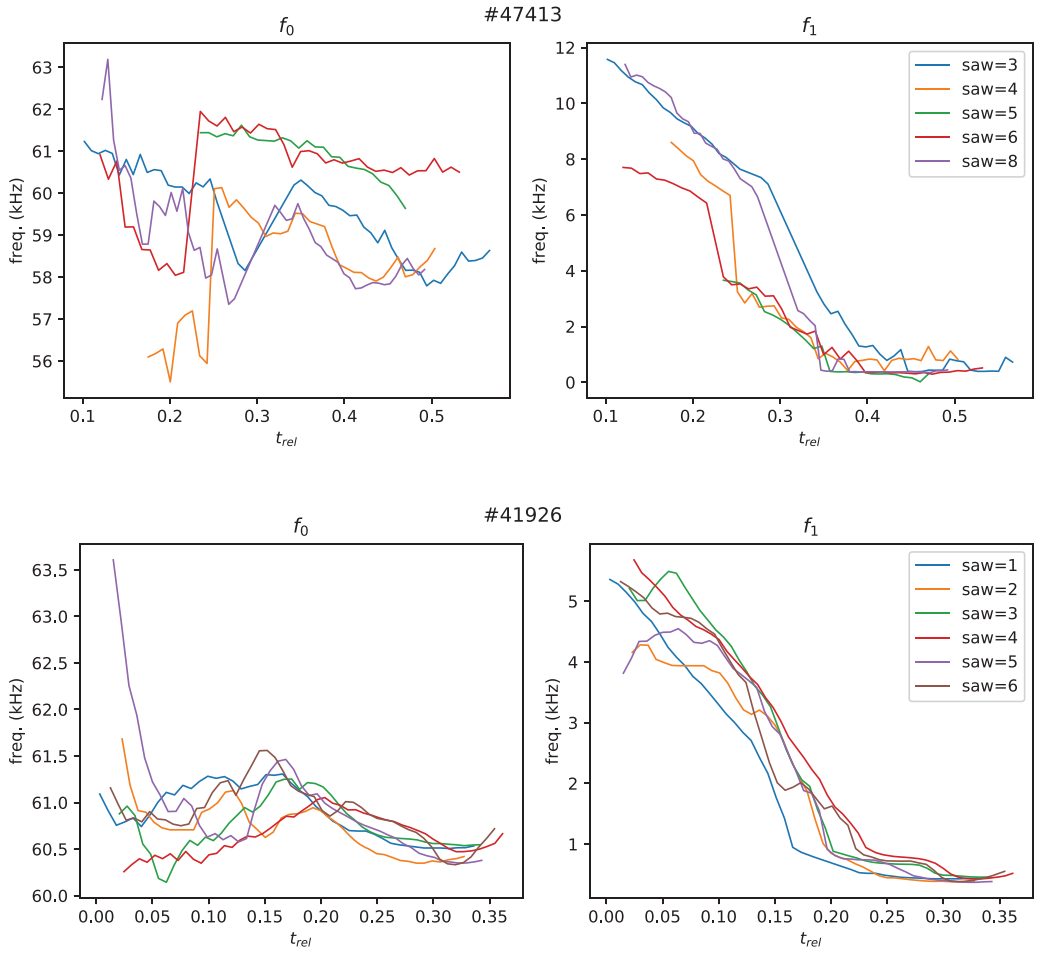

Figure 4. Evolution of fitted parameters from equation (7), in time, for shots #47413 and #41926. t_{rel} is a temporal scale relative to the time between two consecutive sawtooth crashes, where $t_{\mathrm{rel}} = 0$ and $t_{\mathrm{rel}} = 1$ represent the previous and the next crash, respectively.

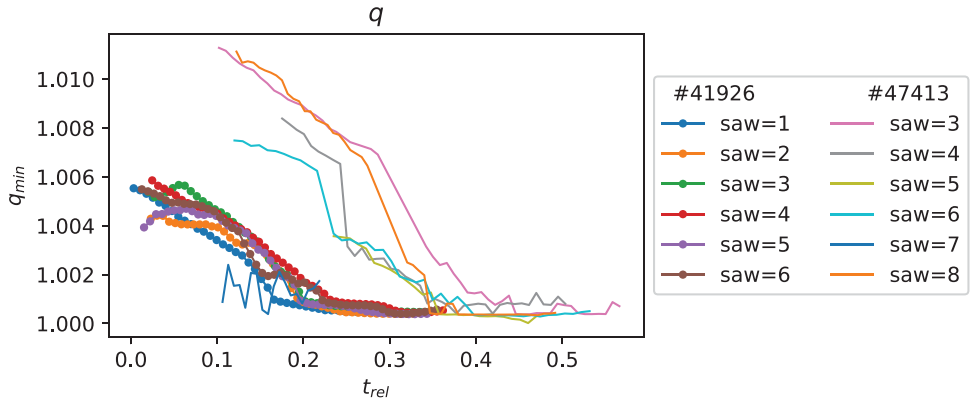

Figure 5. Evolution of q_{min} in time, evaluated from parameter f_1.

6. Reversed q profiles in XTOR-2F sawtooth simulations

The occurrence of a q_{min} indicates a non-monotonic q profile, like in JET reversed shear discharges. The appearance of such q profiles after a sawtooth crash was recently reported and studied by [42], in sawtooth simulations of Ohmic plasmas using the XTOR-2F code [1]. Hence, the evolution of post-crash q profiles depending on the values of the total current in XTOR-2F simulations can be used to examine Tore Supra measurements described in the previous section, even if fast ions are not included in the simulation.

Sustained sawtooth cycles are simulated with the XTOR-2F code in a circular poloidal cross-section. A rescaled Lundquist number $S = 10^7$, which is about an order of magnitude smaller than experimental values in tokamaks, is used to avoid excessive numerical cost. The initial equilibrium used in the simulations is identical to the one described in [43]. In order to model different total current values, the position of the $q = 1$ radius is varied.

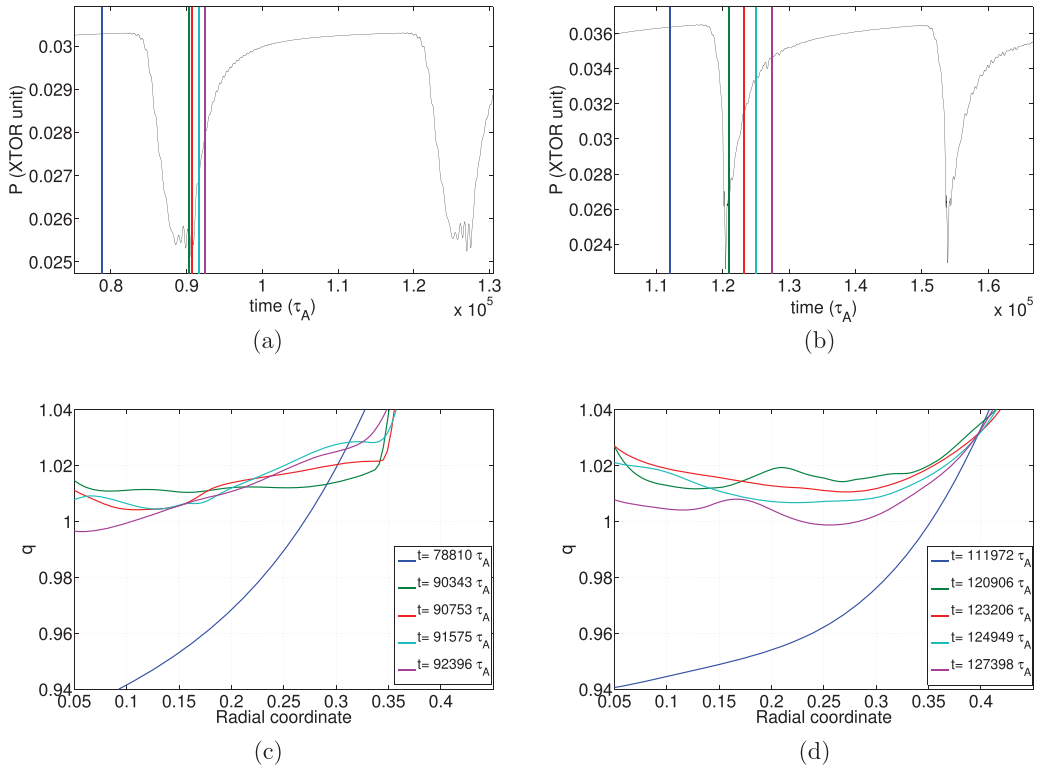

Figure 6. XTOR-2F simulations of sawtooth cycles with the pre-crash $q = 1$ radius located at $\rho_{\rm pol} \simeq 0.27$ (left panel) and $\rho_{\rm pol} \simeq 0.35$ (right panel). Above: time evolution of central pressure ($\rho_{\rm pol} = 0$). Below: evolution of q profiles during sawtooth crash. Each color corresponds to a specific time in the pressure plot above. (*a*) Pressure at plasma center (small core). (*b*) Pressure at plasma center (large core). (*c*) q profile (small core). (*d*) q profile (large core).

Indeed, the increase of the total current flattens the q profile and increases the $q = 1$ radius, since the safety factor value at the edge q_a is inversely proportional to the total current. Figure 6 shows the evolution of the q profiles after a sawtooth crash for the two cases with the $q = 1$ radii before the crash located at $\rho_{\rm pol} \simeq 0.27$ and $\rho_{\rm pol} \simeq 0.35$ respectively. Time units are normalized to the Alfvén time τ_A in the XTOR-2F code. The sawtooth period is approximatively $\tau_{\rm ST} \simeq 3.5 \times 10^4 \tau_A$ for both cases (figures 6(*a*) and (*b*). Note that these sawtooth periods are much smaller than experimental values, due to a rescaled Lundquist number used in XTOR-2F simulations.

For the case with a pre-crash $q = 1$ radius located at $\rho_{\rm pol} \simeq 0.27$, a flattening of the q profile in the core region due to sawtooth crash occurs at $t \simeq 9.0 \times 10^4 \tau_A$ (figure 6(*c*)). Note also that the q profile turns monotonic in less than $2 \times 10^3 \tau_A$ during the following sawtooth ramp phase. However, for the case with a larger pre-crash $q = 1$ radius ($\rho_{\rm pol} \simeq 0.35$), the q profile remains non-monotonic for more than $7 \times 10^3 \tau_A$ after a sawtooth crash at $t \simeq 1.2 \times 10^5 \tau_A$ (figure 6(*d*)). Therefore, XTOR-2F simulations suggest that a reversed shear profile is preserved for a longer time in the case of a larger $q = 1$ radius, which corresponds to the larger total current case. These features are in agreement with the observations described in the previous section, where q profiles remain reversed or flat during a longer time when the plasma current is higher.

The analysis of the measurements with the theoretical model developed in section 5 reveals that the time evolution of $q_{\rm min}$ shown in figure 5 is closely related to the existence of Alfvén modes, since they disappear, in both Tore Supra discharges soon after the value of $q_{\rm min}$ reaches 1.

7. Conclusion and final remarks

The observations in Tore Supra show that with the presence of ICRH heating, MHD modes can appear after sawtooth crashes, in the core region. These modes are in the range of the BAE frequency, shifted by the plasma rotation and modified by the safety factor (q). These modes were not related to other types of Alfvénic modes, like fishbones, because they follow the oscillation of the core temperature, and in Tore Supra usually have lower frequency [40].

This work extends previous works on Tore Supra BAEs that were mainly focused on BAE observations in the last stage of the sawtooth cycle. The observation of an Alfvén cascade is an indication that in these discharges, with a fast ion population generated by ICRH, the q profile is reversed after the crash. This reverse q profile is in agreement with inward radial movement of these Alfvén cascades as previously reported by Guimarães-Filho *et al* [35].

The hypothesis of a reverse q profile with $q_{\rm min}$ slightly larger than 1 in the high current discharge is corroborated by sawtooth simulations with a large $q = 1$ radius, where a reversed q profile develops. This observation also agrees with a very recent publication of q profile measurements in the KSTAR tokamak, with a carefully calibrated MSE diagnostic. They reported that q_0 falls below unity before the crash, and increases up to a value slightly above unity after the crash [44].

XTOR-2F simulations agree that larger plasma current cases can lead to q profiles that stay hollow for a longer period than the lower plasma current cases. Nevertheless, the model used for BAE gives a value of $q_{\min}$ constant in time as soon as it reaches unity (figure 5), whereas XTOR-2F simulations show that $q_{\min}$ decreases below unity during the recovery phase (figure 6), regardless of the value of the plasma current. This is another indication that the model as used is unable to explain the behavior of the modes as $q_{\min}$ reaches unity. Nevertheless, it should be noted that the XTOR-2F code version that was used for this work simulated Ohmic plasmas without the effects of fast ions. Another possible factor is the limitation of the model itself (equation (4)), which cannot describe what happens if $q_{\min}$ is negative—for example—because it evaluates only absolute values.

There are few recorded cases with high current, and the number which were probed with fixed reflectometry for at least the duration of one sawtooth are even smaller. Because Tore Supra was shut down to be upgraded to WEST, we could only work with the existing database, so the required configuration was found in four shots, all showing similar behavior. We expect to perform the same analysis on WEST and other tokamaks.

Acknowledgments

This work is part of the project AMICI funded by the Agence Nationale pour la Recherche (ANR-14-CE32-0004-01), and it was supported with a grant from the Science without Boarders Brazilian program (CNPq grant 235156/2014-0), and FAPESP. We are also thankful for the support from UTFPR and IRFM staff, in particular early discussions with S. Hacquin. One of the authors is very grateful to H. Lütjens for providing the XTOR-2F code.

ORCID iDs

C.H.S. Amador https://orcid.org/0000-0001-7111-0619
J.-H. Ahn https://orcid.org/0000-0002-6786-2823

References

[1] Lütjens H. and Luciani J.F. 2010 *J. Comput. Phys.* **229** 8130–43
[2] Wesson J. and Campbell D. 2004 *Tokamaks* (*International Series of Monographs on Physics*) 3rd edn (Oxford: Clarendon)
[3] von Goeler S., Stodiek W. and Sauthoff N. 1974 *Phys. Rev. Lett.* **33** 1201–3
[4] Kadomtsev B.B. 1975 *Fiz. Plazmy* **1** 710
[5] Porcelli F., Boucher D. and Rosenbluth M. 1996 *Plasma Phys. Control. Fusion* **38** 2163
[6] Zweibel E.G. and Yamada M. 2009 *Annu. Rev. Astron. Astrophys.* **47** 291–332
[7] Kolesnichenko Y.I., Yakovenko Y.V., Anderson D., Lisak M. and Wising F. 1992 *Phys. Rev. Lett.* **68** 3881–4
[8] Hastie R.J. 1998 *Astrophys. Space Sci.* **256** 177–204
[9] Soltwisch H. 1983 *Nucl. Fusion* **23** 1681
[10] Wróblewski D., Huang L.K., Moos H.W. and Phillips P.E. 1988 *Phys. Rev. Lett.* **61** 1724–7
[11] Levinton F.M., Fonck R.J., Gammel G.M., Kaita R., Kugel H.W., Powell E.T. and Roberts D.W. 1989 *Phys. Rev. Lett.* **63** 2060–3
[12] Blum J., Lazzaro E., O'Rourke J., Keegan B. and Stephan Y. 1990 *Nucl. Fusion* **30** 1475
[13] Pecquet A.L., Cristofani P., Mattioli M., Garbet X., Laurent L., Geraud A., Gil C., Joffrin E. and Sabot R. 1997 *Nucl. Fusion* **37** 451
[14] Rice B.W., Nilson D.G., Burrell K.H. and Lao L.L. 1999 *Rev. Sci. Instrum.* **70** 815–20
[15] Dubois M., Sabot R., Pegourie B., Drawin H.W. and Geraud A. 1992 *Nucl. Fusion* **32** 1935
[16] Gill R., Edwards A. and Weller A. 1989 *Nucl. Fusion* **29** 821
[17] Pégourié B. and Dubois M. 1990 *Nucl. Fusion* **30** 1575
[18] Fasoli A., Testa D., Sharapov S., Berk H.L., Breizman B., Gondhalekar A., Heeter R.F., Mantsinen M. and Contributors to the EFDA-JET Workprogramme 2002 *Plasma Phys. Control. Fusion* **44** B159
[19] Fasoli A. *et al* 2007 *Nucl. Fusion* **47** S264–84
[20] Sharapov S.E. *et al* 2004 *Phys. Rev. Lett.* **93** 1–4
[21] Breizman B.N. and Sharapov S.E. 2011 *Plasma Phys. Control. Fusion* **53** 054001
[22] Berk H.L., Borba D.N., Breizman B.N., Pinches S.D. and Sharapov S.E. 2001 *Phys. Rev. Lett.* **87** 185002
[23] Lauber P., Brüdgam M., Curran D., Igochine V., Sassenberg K., Günter S., Maraschek M., García-M Noz M., Hicks N. and ASDEX Upgrade Team 2009 *Plasma Phys. Control. Fusion* **51** 124009–10
[24] Lauber P., Classen I., Curran D., Igochine V., Geiger B., da Graça S., García-Muñoz M., Maraschek M. and McCarthy P. 2012 *Nucl. Fusion* **52** 094007
[25] Breizman B.N., Pekker M.S. and Sharapov S.E. 2005 *Phys. Plasmas* **12** 1–9
[26] Sabot R. *et al* 2009 *Nucl. Fusion* **49** 085033
[27] Fasoli A., Dobbing J.A., Gormezano C., Jacquinot J., Lister J.B., Sharapov S.E. and Sibley A. 1996 *Nucl. Fusion* **36** 258–63
[28] Heidbrink W.W., Ruskov E., Carolipio E.M., Fang J. and Zeeland M.A.V. 1999 *Phys. Plasmas* **6** 1147–61
[29] Chen L. and Zonca F. 2016 *Rev. Mod. Phys.* **88** 1147
[30] Zonca F., Chen L. and Santoro R.A. 1996 *Plasma Phys. Control. Fusion* **38** 2011–28
[31] Gorelenkov N.N., Berk H.L., Fredrickson E., Sharapov S.E. and JET EFDA Contributors 2007 *Phys. Lett. A* **370** 70–7
[32] Nguyen C. *et al* 2009 *Plasma Phys. Control. Fusion* **51** 95002–24
[33] Nguyen C. 2009 Magneto-hydrodynamic activity and energetic particles—application to beta Alfvén eigenmodes *Theses* Ecole Polytechnique X https://pastel.archives-ouvertes.fr/pastel-00005642
[34] Nguyen C., Garbet X., Grandgirard V., Decker J., Guimarães-Filho Z., Lesur M., Lütjens H., Merle A. and Sabot R. 2010 *Plasma Phys. Control. Fusion* **52** 124034
[35] Guimarães-Filho Z.O. *et al* 2011 *Plasma Phys. Control. Fusion* **53** 74012
[36] Sabot R., Sirinelli A., Chareau J.M. and Giaccalone J.C. 2006 *Nucl. Fusion* **46** S685–92
[37] Gil C. *et al* 2009 *Fusion Sci. Technol.* **56** 1219–52
[38] Guimarães-Filho Z.O., Tore Supra and The ASDEX Upgrade Team 2012 *AIP Conf. Proc.* **1478** 129–40
[39] Fenzi C. *et al* 2011 *Nucl. Fusion* **51** 103038
[40] Nguyen C. *et al* 2010 Theoretical and experimental analysis of the destabilization of modes driven by fast particles in Tore Supra *23rd IAEA Fusion Energy Conf. (Daejeon, Republic of Korea, 2010)*
[41] da Graça S. *et al* and The ASDEX Upgrade Team 2012 *Plasma Phys. Control. Fusion* **54** 095014
[42] Ahn J.H. *et al* 2016 *Phys. Plasmas* **23** 052509
[43] Halpern F.D., Lütjens H. and Luciani J.F. 2011 *Phys. Plasmas* **18** 102501
[44] Ko J. 2016 *Rev. Sci. Instrum.* **87** 11E541